Submitted to: *J. Phys. B: At. Mol. Phys.*

LETTER TO THE EDITOR

Field Ionization of C_2H_5I in Supercritical Argon near the Critical Point

C. M. Evans† and G. L. Findley‡

† Department of Chemistry and Biochemistry, Queens College CUNY, Flushing, NY 11367 and Department of Chemistry, Graduate Center CUNY, New York, NY 10016

‡ Department of Chemistry, University of Louisiana at Monroe, Monroe, LA 71209

E-mail: †cevans@forbin.qc.edu, ‡findley@ulm.edu

Abstract. Field ionization of C_2H_5I doped into argon is presented as a function of argon number density along the argon critical isotherm. These data exhibit a decrease in the argon induced shift of the C_2H_5I ionization energy near the critical point similar to recent field ionization measurements of CH_3I/Ar. We show that this decrease is due to the interaction between argon and the quasi-free electron arising from dopant field ionization and is, therefore, independent of the dopant. The energy of the quasi-free electron is calculated in a local Wigner-Seitz model containing no adjustable parameters to within ±0.2% of experiment.

PACS numbers: 33.15.Ry, 34.30.+h, 31.70.-f, 31.70.Dk

Field ionization of molecules doped into perturber fluids provides a means of probing fluid structure as a function of perturber number density. We have recently reported a decrease in the perturber induced shift of the CH_3I ionization energy near the critical point of argon [1]. This decrease contrasts sharply with the increase observed in the density dependent solvatochromic shift of vibrational and UV-visible absorption bands reported by numerous groups [2] in various perturbers. The difference in behavior stems from the nature of the dopant/perturber interactions in the two cases: The density dependent energy shift of vibrational and UV-visible absorption bands is primarily sensitive to the local density and polarizability of the perturbing medium, whereas the density dependent shift of the dopant ionization energy $\Delta_{\rm D}(\rho_{\rm P})$ in dense media can be written as a sum of contributions

$$\Delta_{\rm D}(\rho_{\rm P}) = V_0(\rho_{\rm P}) + P_+(\rho_{\rm P}). \tag{1}$$

In this expression, $P_+(\rho_{\rm P})$ is the shift due to the average polarization of the perturber by the ionic core, $V_0(\rho_{\rm P})$ is the quasi-free electron energy in the perturbing medium, and $\rho_{\rm P}$ is the perturber number density. In modeling the CH_3I ionization energy near the critical point of argon [1], we showed that while $P_+(\rho_{\rm P})$ shifted in a manner similar to that observed for vibrational and UV-visible bands [2], $V_0(\rho_{\rm P})$ did not. Nevertheless, $V_0(\rho_{\rm P})$ could be accurately predicted within a dopant-independent local Wigner-Seitz model at noncritical temperatures [1] and along the critical isotherm [3]. Recent theoretical studies on vibrational and UV-visible bands [4, 5, 6, 7], however, have

shown that the dopant can induce larger density fluctuations in the perturbing medium near the critical point in comparison to density fluctuations in the neat perturber. Since $V_0(\rho_P)$ is dependent upon the local perturber number density [1, 3], this change in local density might lead to a slight dopant dependence in $V_0(\rho_P)$.

In this Letter, we report the field ionization of C_2H_5I high-n Rydberg states in supercritical argon along the critical isotherm near the critical density. These data also show a decrease in the perturber induced shift of the dopant ionization energy near the critical point. The differences between the C_2H_5I results and the previously reported CH_3I/Ar [3] results are shown to arise solely from the average polarization of the perturber by the ionic core (i.e., $P_+(\rho_P)$) and not from $V_0(\rho_P)$. Therefore, for the case in which the number density of the dopant is much less than that of the perturber, dopant effects on the perturber local density fluctuations play no role in the mechanism leading to the density dependence of $V_0(\rho_P)$ around the critical point of the perturber. The local Wigner-Seitz model [1, 3] employed in CH_3I/Ar is used here to predict $V_0(\rho_P)$ and $\Delta_D(\rho_P)$ for the C_2H_5I/Ar system to within $\pm 0.2\%$ of experiment.

C_2H_5I (Sigma, 99.1%) and argon (Matheson Gas Products, 99.9999%) were used without further purification. The absence of trace impurities in the spectral range of interest was verified by the measurement of low density absorption spectra of C_2H_5I, and of both low density and high density absorption spectra of argon. Both the gas handling system and the procedures employed to ensure homogeneous mixing of the dopant and perturber have been described previously [3, 8]. Prior to the introduction of C_2H_5I, the experimental cell and gas handling system were baked to a base pressure of 10^{-8} Torr, and in order to ensure no perturber contamination by the dopant (which was present at a concentration of < 10 ppm), the gas handling system was allowed to return to the low 10^{-7} Torr range before the addition of argon.

Field ionization measurements were preformed using monochromatized synchrotron radiation [8, 9] having a resolution of 0.9 Å (8 meV in the spectral region of interest). The copper experimental cell, capable of withstanding pressures of up to 100 bar, is equipped with entrance and exit MgF_2 windows (1 cm pathlength) and a pair of parallel plate electrodes (stainless steel, 3 mm spacing) oriented perpendicular to the windows [3, 8, 9]. This experimental cell is attached to an open flow cryostat and resistive heater that allowed the temperature to be controlled to within ± 0.2°C. In order to prevent liquid formation in the cell during temperature stabilization, the set point for the critical isotherm was chosen to be -121.5°C, near the argon critical temperature of -122.3°C. The intensity of the synchrotron radiation exiting the monochromator was monitored by measuring the current across a Ni mesh intercepting the beam prior to the experimental cell. All photoionization measurements were normalized to this current. Field ionization spectra were also energy corrected for the effects of both the low field F_L and high field F_H (used to generate the field ionization measurement [9]) by $I_0(\rho_P) = I_F(\rho_P) + c_D(F_L^{1/2} + F_H^{1/2})$, where $I_F(\rho_P)$ is the zero-field dopant ionization energy, $I_F(\rho_P)$ is the dopant ionization energy perturbed by the electric field, and $c_D = 3.0 \pm 0.5 \times 10^{-4}$ cm$^{1/2}$ V$^{-1/2}$ for C_2H_5I [3]. For all field ionization measurements reported here, $F_L = 1667$ V/cm and $F_H = 8333$ V/cm.

Figure 1a presents the argon induced shift of the C_2H_5I ionization energy $\Delta_{EtI}(\rho_{Ar})$ near the critical isotherm of argon, in comparison to that for noncritical isotherms [3]. These data show a clear decrease in the density dependent shift of $\Delta_{EtI}(\rho_{Ar})$ near the argon critical density ($\rho_{Ar} = 8.0 \times 10^{21}$ cm^{-3}) similar to that observed from field ionization measurements of the CH_3I/Ar system (cf. figure 1b) [1]. From a careful perusal of figure 1, one can see that the energy shift for the noncritical

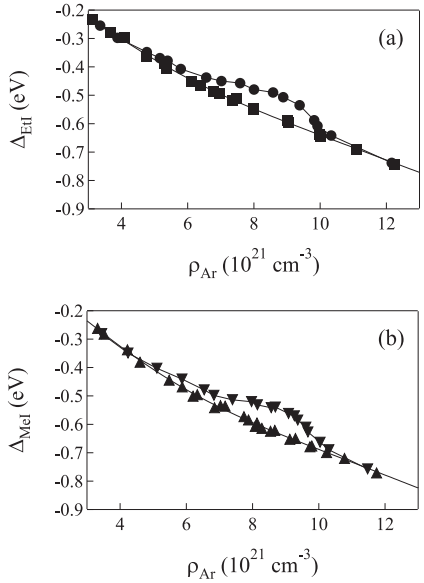

Figure 1. The experimental argon induced shift of (a) the C_2H_5I ionization energy $\Delta_{EtI}(\rho_{Ar})$ and (b) the CH_3I ionization energy $\Delta_{MeI}(\rho_{Ar})$ plotted as a function of argon number density ρ_{Ar} at (■, ▲) various noncritical temperatures [3] and near (●, ▼ [1]) the critical temperature of Ar. The solid lines are provided as a visual aid.

isotherms is slightly smaller for the C_2H_5I/Ar system in comparison to the CH_3I/Ar system, and that the change in the energy shift due to critical effects is also smaller. In order to determine if these differences arise from $V_0(\rho_P)$, the average ion/perturber polarization energy $P_+(\rho_P)$ must be evaluated and subtracted from $\Delta_D(\rho_P)$. For this system, $P_+(\rho_P)$ was calculated using [1, 3]

$$P_+(\rho_P) = -4\pi\rho_P \int_0^\infty g_{PD}(r)\, w_+(r)\, r^2\, dr, \tag{2}$$

where $g_{PD}(r)$ is the perturber/dopant radial distribution function and $w_+(r)$ is the perturber/ion interaction potential [1, 3, 9]. Since $w_+(r)$ incorporates induced dipole interactions in the perturbing medium, the perturber/perturber radial distribution function $g_{PP}(r)$ is also involved in determining $P_+(\rho_P)$. As was the case for CH_3I/Ar [1, 3], the radial distribution functions $g_{PD}(r)$ and $g_{PP}(r)$ were computed from the coupled Percus-Yevick integral equations [3, 9] with a Lennard-Jones 6-12 potential employed for the Ar/Ar interaction and a modified Stockmeyer potential written in Lennard-Jones 6-12 form [3] employed for the C_2H_5I/Ar interaction. (The Lennard-Jones 6-12 parameters [3] were $\sigma_{PP} = 3.409$ Å and $\varepsilon_{PP}/k_B = 119.5$ K for the Ar/Ar potential, and $\sigma_{PD} = 4.394$ Å and $\varepsilon_{PD}/k_B = 139.1$ K for the C_2H_5I/Ar potential ($k_B \equiv$ Boltzmann's constant).) The average ion/perturber polarization energies $P_+(\rho_{Ar})$ for C_2H_5I/Ar calculated from equation (2) are plotted versus argon number density in figure 2a, along with $P_+(\rho_{Ar})$ for CH_3I/Ar [1] in figure 2b. Subtracting $P_+(\rho_{Ar})$ from $\Delta_{EtI}(\rho_{Ar})$ leads to the experimental values of $V_0(\rho_{Ar})$ for the C_2H_5I/Ar critical isotherm data, which are presented in figure 3 and compared to the noncritical isotherm data for C_2H_5I/Ar [3] as well as the critical isotherm data for CH_3I/Ar [1]. Clearly, $V_0(\rho_{Ar})$ along the critical isotherm is the same for both the CH_3I/Ar and C_2H_5I/Ar systems

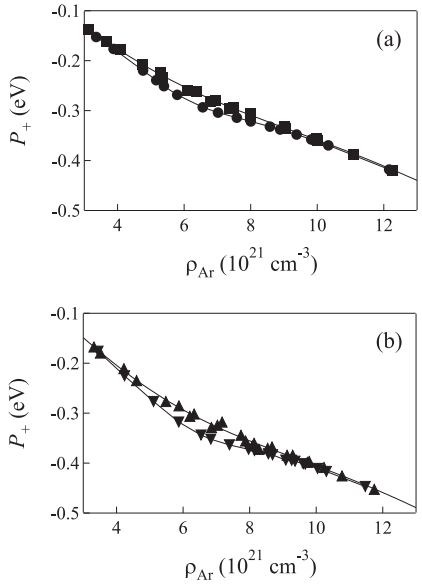

Figure 2. The average ion/perturber polarization energy $P_+(\rho_{Ar})$ of (a) C_2H_5I and (b) CH_3I plotted as a function of argon number density ρ_{Ar} at (■, ▲) various noncritical temperatures [3] and near (●, ▼ [1]) the critical temperature of Ar. The solid lines are provided as a visual aid.

and, therefore, shows no dopant dependence.

Since $V_0(\rho_{Ar})$ for the C_2H_5I/Ar system is independent of the dopant, we can model $V_0(\rho_{Ar})$ within a recently presented local Wigner-Seitz treatment [1, 3]. This model begins with a one-electron Schrödinger equation for the potential $V(r)$ that describes the interaction between the quasi-free electron and the neat fluid. As in the original Springett, Jortner and Cohen (SJC) model [10], we assume that $V(r)$ is spherically symmetric about the perturber, and that (neglecting fluctuations) it has an average translational symmetry. However, our model does not assume that the average distance between atoms in a dense fluid can be determined by dividing the volume into spheres defined by the Wigner-Seitz radius [10] obtained from the bulk number density. In dense fluids, one does not have a uniform distribution of perturbers because of perturber/perturber interactions, and the translational symmetry boundary condition must reflect this nonuniformity. This refinement necessitates the replacement of the bulk number density ρ_P employed in the SJC model [10] with the local number density $\rho_P(r)$, which is obtained from $g_{PP}(r)$ via [11, 12]

$$\rho_P(r) = g_{PP}(r)\ \rho_P\ . \tag{3}$$

Since the maximum of $\rho_P(r)$ gives the density of the first solvent shell, this value more closely reflects the actual number density in the neighborhood of any given perturber. In this case, then, the translational symmetry is defined by a local Wigner-Seitz radius [1, 3]

$$r_\ell = \sqrt[3]{\frac{3}{4\ \pi\ g_{max}\ \rho_P}}\ , \tag{4}$$

where g_{max} is the maximum of the radial distribution function. The local Wigner-Seitz radius r_ℓ, therefore, represents one-half the average spacing between rare gas atoms

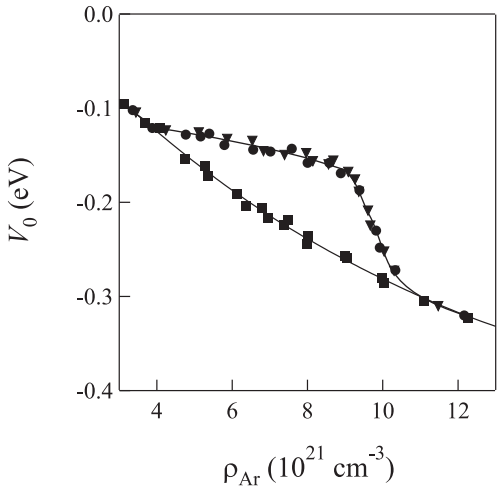

Figure 3. $V_0(\rho_{\rm Ar})$, determined from equation (1) by subtracting $P_+(\rho_{\rm Ar})$ in figure 2a from the experimentally determined argon induced shift of the C_2H_5I ionization energy $\Delta_{\rm EtI}(\rho_{\rm Ar})$ in figure 1a, plotted as a function of argon number density $\rho_{\rm Ar}$ at (■) various noncritical temperatures [3] and near (●) the critical temperature of Ar. (▼) represents $V_0(\rho_{\rm Ar})$ for CH_3I/Ar near the critical temperature of Ar [1] and is provided for comparison. The solid lines are provided as a visual aid.

in the first solvent shell. As in the SJC model [10], we assume that $V(r)$ is divided into two parts: an attractive electron/perturber polarization energy $P_-(\rho_{\rm P})$ and a repulsive atomic pseudopotential $V_a(r)$. We calculate the attractive electron/perturber polarization energy $P_-(\rho_{\rm P})$ in a manner similar to that given for the ion polarization potential $P_+(\rho_{\rm P})$ in equation (2), but with an interaction potential originally proposed by Lekner [13],

$$w_-(r_1,\ldots,r_N) = -\frac{1}{2}\,\alpha_{\rm P}\,e^2\,\sum_i^N r_i^{-4}\,f_-(r_i)\,. \tag{5}$$

In equation (5), $\alpha_{\rm P}$ is the polarizability of the perturber, e is the electron charge, and $f_-(r)$ is a screening function given by

$$f_-(r) = 1 - \alpha_{\rm P}\pi\rho_{\rm P}\int_0^\infty \frac{1}{s^2}\,g_{\rm PP}(s)\,ds\int_{|r-s|}^{r+s}\frac{1}{t^2}\,f_-(t)\,\theta(r,s,t)\,dt\,, \tag{6}$$

where $\theta(r,s,t)$ is defined by

$$\theta(r,s,t) = \frac{3}{2s^2}\,(s^2+t^2-r^2)(s^2-t^2+r^2) + (r^2+t^2-s^2)\,, \tag{7}$$

and where the integration variables s and t represent the distance between the atom of interest and all other perturber atoms. The ensemble average electron/perturber polarization energy can then be obtained from [1, 3]

$$P_-(\rho_{\rm P}) = -4\pi\rho_{\rm P}\int_0^\infty g_{\rm PP}(r)\,w_-(r)\,r^2\,dr\,. \tag{8}$$

The potential $V(r)$ in the one-electron Schrödinger equation therefore becomes $V(r) = V_a(r) + P_-(\rho_{\rm P})$, where $P_-(\rho_{\rm P})$ is a constant for a fixed perturber number

density. As in the SJC treatment [10], we define $V_a(r)$ as a hard core potential (i.e., $V_a(r) = 0$ for $r > r_h$ and $V_a(r) = \infty$ for $r < r_h$, where r_h is the hard core radius), but we set r_h equal to the absolute value of the scattering length A of the perturber. Finally, a phase shift is introduced to reflect the fact that outside the first solvent shell the quasi-free electron wavefunction can also scatter off the rare gas atoms contained within the solvent shell. For s-wave scattering, and in the limit of small k_0, this phase shift is given by $\eta\pi$, where η is the phase shift amplitude [14]. Incorporating this phase shift into the solution to the one-electron Schrödinger equation under the boundary conditions

$$\psi_0(|A|) = 0 \,, \qquad \left(\frac{\partial \psi_0}{\partial r}\right)\Bigg|_{r=r_\ell} = 0 \,. \tag{9}$$

yields the wavevector equation for the quasi-free electron:

$$tan[k_0(r_\ell - |A|) + \eta\pi] = k_0 \, r_\ell \,. \tag{10}$$

In this model, η is a perturber dependent (but dopant independent) parameter that is evaluated from the field ionization and/or photoconduction data for $V_0(\rho_{\rm P})$ from the noncritical isotherm experiments [3]. Once the thermal kinetic energy of the quasi-free electron is included, $V_0(\rho_{\rm P})$ becomes

$$V_0(\rho_{\rm P}) = E_k + P_-(\rho_{\rm P}) + \frac{3}{2}k_B T \,, \qquad E_k = \frac{(\hbar k_0)^2}{2m} \tag{11}$$

where k_0 is evaluated from equation (10). It is important to note here that E_k inherits an implicit temperature dependence from the local Wigner-Seitz radius, a dependence that is absent in the SJC model [10].

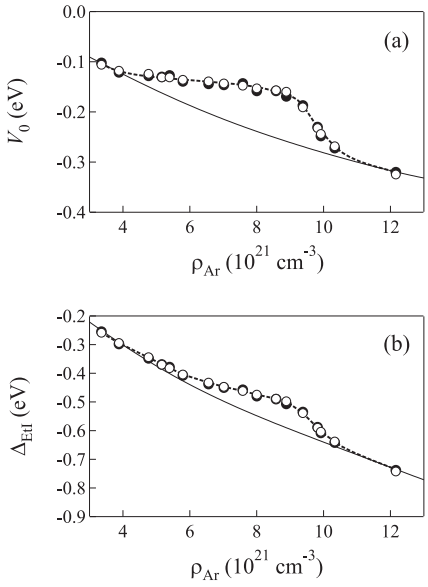

Figure 4. Comparison of experiment (•) and calculation (○) for (a) the energy of the quasi-free electron in argon $V_0(\rho_{\rm Ar})$, and for (b) the argon induced shift of the C_2H_5I ionization energy $\Delta_{\rm EtI}(\rho_{\rm Ar})$, plotted as a function of argon number density $\rho_{\rm Ar}$ for an isotherm ($-121.5°$C) near the argon critical isotherm. The lines are provided as a visual aid. The solid line is a nonlinear least squares fits (using a seventh order polynomial function) to the noncritical isotherm data [3].

Figure 4a presents $V_0(\rho_{\mathrm{Ar}})$ obtained from equation (11), with $\eta = 0.40$ [1, 3] and $A = -0.82$ Å [10], for the critical isotherm (open markers), in comparison to the experimentally determined values (solid markers) [cf. figure 3]. (A nonlinear least squares fit to the noncritical isotherm data [3] (solid line) is included in figure 4a as an aid to the eye.) Clearly, the calculated $V_0(\rho_{\mathrm{Ar}})$ closely matches experiment, with a scatter of $\pm 0.2\%$ of experiment that easily falls within the experimental error of ± 0.02 eV. Similarly, figure 4b presents the calculated $\Delta_{\mathrm{EtI}}(\rho_{\mathrm{Ar}})$ along the critical isotherm (open markers), using $P_+(\rho_{\mathrm{Ar}})$ obtained from equation (2) [cf. figure 2a] and $V_0(\rho_{\mathrm{Ar}})$ obtained from equation (11), in comparison to the experimentally determined values (solid markers) [cf. figure 1]. (A nonlinear least squares fit to the noncritical isotherm data [3] (solid line) is also included in figure 4b as an aid to the eye.) Again, the calculated $\Delta_{\mathrm{EtI}}(\rho_{\mathrm{Ar}})$ closely matches experiment, with a scatter of $\pm 0.2\%$ of experiment that easily falls within the overall experimental error of ± 0.02 eV. It is important to note that there are no adjustable parameters in this model for the critical isotherm data, since η was determined from the noncritical isotherm data [3]. Future studies will focus on a systematic assessment of the perturber dependence of the phase shift parameter η

Finally, figure 5 presents a summary of the calculations necessary to model $V_0(\rho_{\mathrm{Ar}})$ using equation (11). One can clearly see in figure 5a that $P_-(\rho_{\mathrm{Ar}})$ shows a slight increase in the argon induced shift near the critical point, similar to the behavior observed for vibrational and UV-visible absorption bands [2]. However, as shown in figure 5b, the zero-point kinetic energy E_k increases by approximately 0.1 eV along the critical isotherm near the critical point. (It is interesting to note that the critical isotherm turning points that bound the saddle point in the argon phase

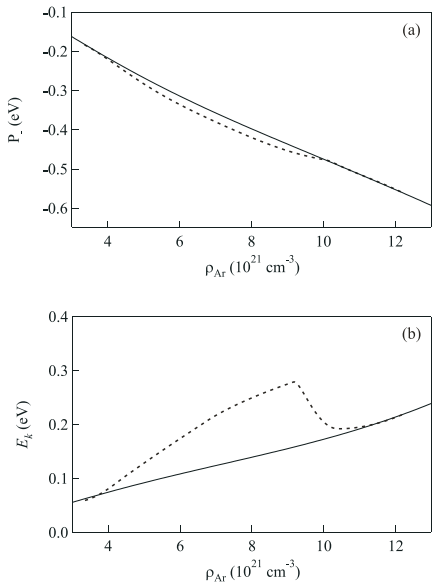

Figure 5. Summary of the calculations necessary to model $V_0(\rho_{\mathrm{Ar}})$ from equation (11) on (– –) an isotherm (−121.5°C) near the argon critical isotherm and on (—) noncritical isotherms. (a) The average electron/perturber polarization energy $P_-(\rho_{\mathrm{Ar}})$, and (b) the zero-point kinetic energy of the quasi-free electron E_k plotted as a function of argon number density ρ_{Ar}.

diagram coincide with the number densities that delimit the deviations of E_k from the noncritical isotherm values.) This increase in the kinetic energy of the quasi-free electron, which results from critical point fluctuations that are reflected in variations in the radial distribution function in the critical point region, is a consequence of the decreasing value of r_ℓ: as the boundary condition for the quasi-free electron wavefunction decreases, the kinetic energy of the quasi-free electron must increase. This result may well have a bearing on the changes in reactivity [2, 15, 16] and product distribution [2, 15, 16] observed in chemical reactions conducted in supercritical fluids. Furthermore, the increase in E_k is the determining factor for the observed decrease in the $V_0(\rho_{\mathrm{Ar}})$ shift near the critical point of argon (cf. figure 3).

Acknowledgments

We are grateful to Dr. Ruben Reininger (University of Wisconsin Synchrotron Radiation Center) for many helpful discussions. We thank Luxi Li (Queens College) for her assistance in the calculations contained in figures 4-5. The experimental measurements reported here were performed at the University of Wisconsin Synchrotron Radiation Center (NSF DMR-0084402). This work was supported by grants from the Petroleum Research Foundation (41378-G6) and from the Professional Staff Congress - City University of New York (60073 - 34 35).

References

[1] Evans C M and Findley G L 2005 *Chem. Phys. Lett.* **410** 242.
[2] Tucker S C 1999 *Chem. Rev.* **99** 391 and references therein.
[3] Evans C M and Findley G L 2005 *Phys. Rev. A* **72** 054508.
[4] Egorov S A 2002 *Chem. Phys. Lett.* **354** 140.
[5] Egorov S A and Skinner J L 2000 *J. Phys. Chem. A* **104** 483.
[6] Egorov S A 2000 *J. Chem. Phys.* **113** 1950.
[7] Egorov S A 2002 *J. Chem. Phys.* **116** 2004.
[8] Evans C M, Scott J D and Findley G L 2002 *Rec. Res. Dev. Chem. Phys.* **3** 351.
[9] Al-Omari A K, Atlmann K N and Reininger R 1996 *J. Chem. Phys.* **105** 1305.
[10] Springett B E, Jortner J and Cohen M H 1968 *J. Chem. Phys.* **48** 2720.
[11] Attard P 1989 *J. Chem. Phys.* **91** 3072.
[12] Attard P 1989 *J. Chem. Phys.* **91** 3083.
[13] Lekner J 1967 *Phys. Rev.* **158** 130.
[14] Calogero F 1967 *Variable Phase Approach to Potential Scattering* (New York: Academic Press).
[15] Kajimoto O 1999 *Chem. Rev.* **99** 355 and references therein.
[16] Tucker S C and Maddox M W 1998 *J. Phys. Chem. B* **102** 2437.